

Color Correction of Baby Images for Cyanosis Detection

Nur Fatihah Binti Azmi^{1,3}, Frank Delbressine¹, Loe Feijs¹, and Sidarto Bambang Oetomo²

¹ Department of Industrial Design, Eindhoven University of Technology, Eindhoven, The Netherlands.

² Department of Neonatology, Maxima Medical Center, Veldhoven, The Netherlands

³ Faculty of Electronics and Computer Engineering,, Universiti Teknikal Malaysia Melaka, 76100, Melaka, Malaysia
n.f.b.azmi@tue.nl

Abstract. An accurate assessment of the bluish discoloration of cyanosis in the newborn baby's skin is essential for the doctors when making a comprehensive evaluation or a treatment decision. To date, midwives employ the score of APGAR to note any occurrence of discoloration on skin among newborn babies. However, a technique to detect the condition of skin cyanosis among infants is yet to be developed, especially for quantitative analysis. Furthermore, a viable yardstick is absent for evaluation purposes in training sessions. Hence, this study proposes a method to detect and to quantify skin cyanosis based on images of newborns by using an algorithm developed to analyze correction of color via MacBeth Colorchecker. This proposed system has three steps: i) selecting cyanosis areas from images, ii) correcting color via an algorithm to attune images, and iii) generating a database of cyanosis CIE $L^*a^*b^*$ (CIELAB) values. This proposed method calculates color error with ΔE^* via via MacBeth Colorchecker that has 24 patches of color to find its actual value with X-Rite Ci60 spectrophotometer, especially before and after applying correction for color. This proposed method to detect cyanosis allows modification of images with minimal effect upon image quality, thus assuring the viability in detecting and ascertaining values of CIELAB for skin cyanosis. Besides, this study hopes to use the outcomes from CIELAB of images related to cyanosis among infants in order to develop a manikin of baby with cyanosis that is high in fidelity in upcoming studies. This study is not associated to clinical purposes.

Keywords: cyanosis, neonatal care, medical training, CIELAB, color correction, color calibration, medical image, image processing, linear least square.

1 INTRODUCTION

Cyanosis in newborns is referring to the blue discoloration of the skin and mucous membranes that can be recognised all over the body especially around the mouth and the lips [19]. In fact, the occurrence of cyanosis in infants needs critical assessment and diagnosis by the medical team since this color change of a baby's skin is one of the most significant clinical signs during the first minutes after birth and severe disease in general [21, 14]. As such, approximately 3-5 g/dL of deoxygenated hemoglobin is

2 Azmi *et al.*

required to confirm the occurrence of cyanosis among new infants via clinical evaluation. Hence, cyanosis can be diagnosed by determining the saturation level of oxygen from the total amount of hemoglobin. Besides, a new infant is diagnosed with cyanosis when the saturation level of oxygen determined via pulse oximetry is extremely low at 78-83% with normal hemoglobin count [15]. Since cyanosis among new infants are reflective of early sign for lung disease and congenital heart [17], it is essential to determine the occurrence of cyanosis with viable tests and to prescribe effective treatment upon accurate diagnosis. Unfortunately, substantial variations among doctors seem to mislead accurate diagnosis of cyanosis [7]. Thus, in order to accurately detect the case of cyanosis among newborns, a more effective training among future physicians can take place by incorporating cyanosis-affected infant manikins. Recently, the adoption of digital photography in many clinical domains is considered as an acceptable tool as it offers manual or automatic adjustments to correct the color distortions. Apart from that, digital images offer both quantitative and qualitative information for a more detailed evaluation, in comparison to the non-digital conventional approach [19]. It is important to acknowledge the several factors that influence the color of the baby's skin, which could perhaps due to shade of light, certain camera angles towards the infant, as well as influence of other colored items around the infant [8], thus presenting a challenge in accurately diagnosing cyanosis. Therefore, a system for correction of color is needed in order to calibrate and determine the real color of the image.



Fig. 1. An instance of infant's image with the calibrated MacBeth Colorchecker placed next to the infant (the test subject). Note that in this photograph, the lighting condition in the operation room (OR) is unknown, and a non-calibrated digital camera is used

An instance of a photography setup for infant is illustrated in Figure 1. In the attempt to correct these factors, the MacBeth Colorchecker is incorporated in the process

of color correction [2], whereby this tool is positioned next to an infant when pictures are snapped. Unfortunately, as portrayed in the image given, absence of lighting information in the Operation Room (OR) and usage of uncalibrated digital camera demand a reliable process for color correction in accurately diagnosing cyanosis. With that, his work proposes a system for color correction enables the quantifying of cyanosis color of a newborn in images. Hence, the CIELAB, as reckoned by the International Commission on Illumination, is embedded in this system for its description of colors visible to the human eye [22] to quantify the color differences between any two colors. Additionally, this proposed system could be employed to develop a database comprised of color images. In precise, the objective of this work is to design and to develop an infant manikin with controlled cyanosis for clinical training purposes.

1.1 Color Space of Cyanosis Baby Images

This CIELAB, particularly for evaluation of skin color assessment can provide an objective measure for clinicians to make scores for diagnostics of skin color ranges [22, 20] to accurately diagnose and provide effective treatments for cyanosis, pallor, blanch re-sponse, and jaundice [10]. With that, this particular work looks into quantifying the difference of discoloration in a newborn baby's skin color under unknown illumination. The distance between any two colors in CIELAB space is measured as the Euclidean distance in three- dimensional (3D) [10]. In Figure 2, which appears to be courtesy of [1] portrays lighting denoted by the z-axis within the coordinates of Cartesian that reflect 0 for black, while 100 for white, while $R(\lambda)$ is retained at 1. Meanwhile, $+a^*$ axis represents the amount of purplish red, while the $-a^*$ represents the amount of green. $+b^*$ axis represents the amount of yellow and the $-b^*$ represents the amount of blue. The possible values fall between 0 and +100 for lighting, L^* , while -100 and +100 for a^* and b^* , respectively [13].

1.2 Structure of The System

The proposed system to detect cyanosis among newborns embeds two functions, which are: i) determination of color correction matrix (CCM) in order to correct an image, and ii) application of color correction by selecting the region of interest (ROI). Figure 3 presents the system flowchart and further description of the processes is detailed as follows:

Initially, an infants photograph, captured along with MacBeth colorchecker is uploaded into a software program. Next, the colorchecker image is extracted from the infant's image. After that, mean value of CIELAB for each color patch in the colorchecker is identified by applying the image processing module in Wolfram Mathematicas 11.0 module for image processing [5]. Here, the measured colors of each L^* , a^* and b^* that correspond to the 24 color patches in the colorchecker are termed as C_{ccp} . The C_{ccp} refers to the matrix of 3 columns multiplied by 24 rows that are found in the squares of the X-Rite type colorchecker.

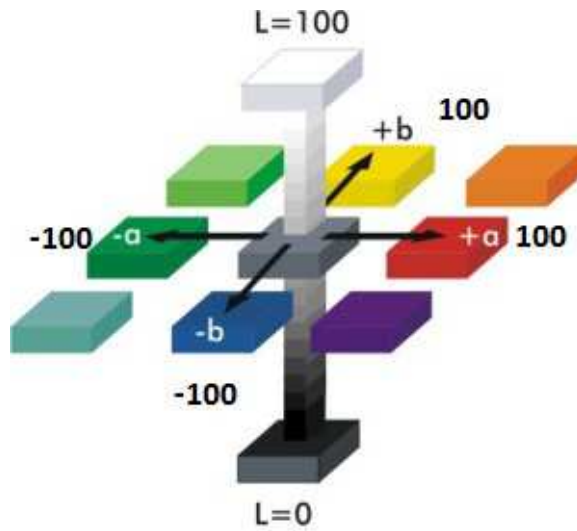


Fig. 2. $L^*a^*b^*$ axes for the CIELAB color space

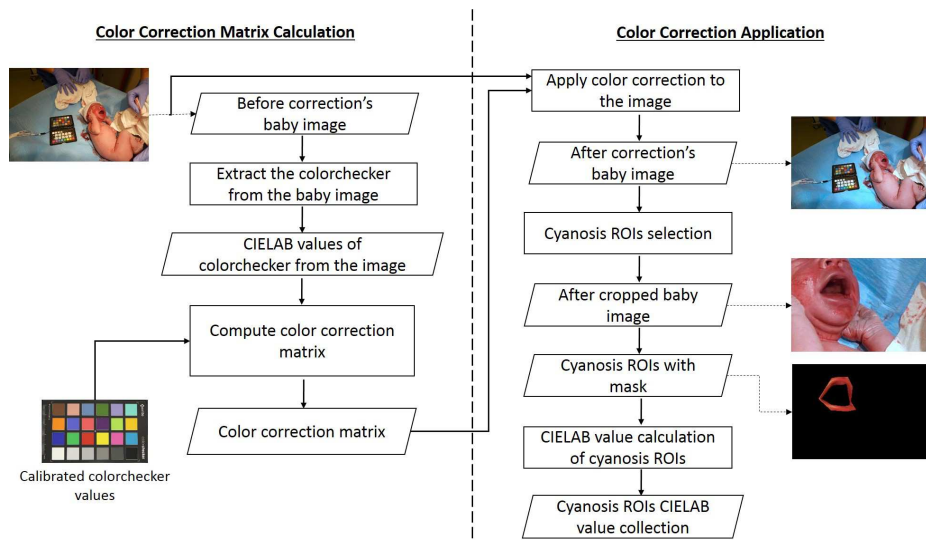


Fig. 3. A block diagram of cyanosis detection system. The first task is color correction matrix calculation and the second part of the system is applying color correction algorithm to the images

As for the three columns, they reflect the values of L^* , a^* and b^* as given in (1).

$$C_{\text{ccp}} = \begin{bmatrix} L^*_{\text{ccp}[1]} & a^*_{\text{ccp}[1]} & b^*_{\text{ccp}[1]} \\ L^*_{\text{ccp}[2]} & a^*_{\text{ccp}[2]} & b^*_{\text{ccp}[2]} \\ \dots & \dots & \dots \\ \dots & \dots & \dots \\ L^*_{\text{ccp}[24]} & a^*_{\text{ccp}[24]} & b^*_{\text{ccp}[24]} \end{bmatrix} \quad (1)$$

A portable spectrophotometer type X-Rite Ci60 [2] was employed to determine the values of colors in MacBeth colorchecker. The value provides the reference color value for the estimation of the relationship between the color value in the image and the actual color. Next, the lighting tool was set at D65, which is a standard of CIE to reflect daylight condition with white reference and the measurement values are presented in CIELAB values with a 10° standard observer. Meanwhile, the measured color matrix for 24 rows and 3 columns of C_{ref} is constructed similarly as in C_{ccp} . The C_{ref} refers to as follows:

$$C_{\text{ref}} = \begin{bmatrix} L^*_{\text{ref}[1]} & a^*_{\text{ref}[1]} & b^*_{\text{ref}[1]} \\ L^*_{\text{ref}[2]} & a^*_{\text{ref}[2]} & b^*_{\text{ref}[2]} \\ \dots & \dots & \dots \\ \dots & \dots & \dots \\ L^*_{\text{ref}[24]} & a^*_{\text{ref}[24]} & b^*_{\text{ref}[24]} \end{bmatrix} \quad (2)$$

Color Correction Matrix Calculation: This section elaborates the calculation of optimal CCM via automated linear least square [23]. The CCM is a 3×3 matrix, mapping the measured colorchecker values, C_{ccp} , into the actual values of colorchecker reference, C_{ref} . In other words, the relationship between the reference values and the distorted value is mentioned below where T is the matrix transpose:

$$[C_{\text{ref}}]^T = \text{CCM} \cdot [C_{\text{ccp}}]^T \quad (3)$$

The CCM is portrayed in (4)

$$\text{CCM} = \begin{bmatrix} a_{1,1} & a_{1,2} & a_{1,3} \\ a_{2,1} & a_{2,2} & a_{2,3} \\ a_{3,1} & a_{3,2} & a_{3,3} \end{bmatrix} \quad (4)$$

where, dual subscripts of the matrix refer to the position of rows and columns, respectively. Thus, for all the color patches indexes, i , where $1 \leq i \leq 24$, the transformed pixel color is a linear mapping of the distorted L^* , a^* and b^* . For example, color in the i th index for the modified C_{ref} can be expressed as:

$$\begin{aligned} L^*_{\text{ref}[i]} &= a_{1,1} \cdot L^*_{\text{ccp}[i]} + a_{1,2} \cdot a^*_{\text{ccp}[i]} + a_{1,3} \cdot b^*_{\text{ccp}[i]}, \\ a^*_{\text{ref}[i]} &= a_{2,1} \cdot L^*_{\text{ccp}[i]} + a_{2,2} \cdot a^*_{\text{ccp}[i]} + a_{2,3} \cdot b^*_{\text{ccp}[i]}, \\ b^*_{\text{ref}[i]} &= a_{3,1} \cdot L^*_{\text{ccp}[i]} + a_{3,2} \cdot a^*_{\text{ccp}[i]} + a_{3,3} \cdot b^*_{\text{ccp}[i]} \end{aligned} \quad (5)$$

6 Azmi *et al.*

Hence, the optimal solution of CCM for this proposed system derives from the equations of least square, as follows:

$$\begin{aligned}
 \begin{bmatrix} L^*_{\text{ref}[1]} \\ \vdots \\ L^*_{\text{ref}[24]} \end{bmatrix} &= \begin{bmatrix} L^*_{\text{ccp}[1]} & a^*_{\text{ccp}[1]} & b^*_{\text{ccp}[1]} \\ L^*_{\text{ccp}[2]} & a^*_{\text{ccp}[2]} & b^*_{\text{ccp}[2]} \\ \dots & \dots & \dots \\ \dots & \dots & \dots \\ L^*_{\text{ccp}[24]} & a^*_{\text{ccp}[24]} & b^*_{\text{ccp}[24]} \end{bmatrix} \cdot \begin{bmatrix} a_{1,1} \\ a_{1,2} \\ a_{1,3} \end{bmatrix} \\
 \begin{bmatrix} a^*_{\text{ref}[1]} \\ \vdots \\ a^*_{\text{ref}[24]} \end{bmatrix} &= \begin{bmatrix} L^*_{\text{ccp}[1]} & a^*_{\text{ccp}[1]} & b^*_{\text{ccp}[1]} \\ L^*_{\text{ccp}[2]} & a^*_{\text{ccp}[2]} & b^*_{\text{ccp}[2]} \\ \dots & \dots & \dots \\ \dots & \dots & \dots \\ L^*_{\text{ccp}[24]} & a^*_{\text{ccp}[24]} & b^*_{\text{ccp}[24]} \end{bmatrix} \cdot \begin{bmatrix} a_{2,1} \\ a_{2,2} \\ a_{2,3} \end{bmatrix} \\
 \begin{bmatrix} b^*_{\text{ref}[1]} \\ \vdots \\ b^*_{\text{ref}[24]} \end{bmatrix} &= \begin{bmatrix} L^*_{\text{ccp}[1]} & a^*_{\text{ccp}[1]} & b^*_{\text{ccp}[1]} \\ L^*_{\text{ccp}[2]} & a^*_{\text{ccp}[2]} & b^*_{\text{ccp}[2]} \\ \dots & \dots & \dots \\ \dots & \dots & \dots \\ L^*_{\text{ccp}[24]} & a^*_{\text{ccp}[24]} & b^*_{\text{ccp}[24]} \end{bmatrix} \cdot \begin{bmatrix} a_{3,1} \\ a_{3,2} \\ a_{3,3} \end{bmatrix}
 \end{aligned} \tag{6}$$

Using the MoorePenrose pseudoinverse [12], 3 separate linear fit estimations, one for each row of the matrix of the CCM is calculated. Therefore, upon obtaining the correction value of CIELAB, the value of C_{real} in any of the chosen i th, j th pixel within the images could be determined as given in the following:

$$[C_{\text{real}}]^T = \text{CCM} \cdot [C_{\text{pic}}]^T \tag{7}$$

whereby C_{pic} refers to the following:

$$C_{\text{pic}} = \begin{bmatrix} L^*_{\text{pic}[1]} & a^*_{\text{pic}[1]} & b^*_{\text{pic}[1]} \\ L^*_{\text{pic}[2]} & a^*_{\text{pic}[2]} & b^*_{\text{pic}[2]} \\ \dots & \dots & \dots \\ \dots & \dots & \dots \\ L^*_{\text{pic}[n]} & a^*_{\text{pic}[n]} & b^*_{\text{pic}[n]} \end{bmatrix} \tag{8}$$

In fact, the value of C_{real} matrix can be determined similarly is constructed in the same way as the C_{ccp} and C_{ref} as given below:

$$C_{\text{real}} = \begin{bmatrix} L^*_{\text{real}[1]} & a^*_{\text{real}[1]} & b^*_{\text{real}[1]} \\ L^*_{\text{real}[2]} & a^*_{\text{real}[2]} & b^*_{\text{real}[2]} \\ \dots & \dots & \dots \\ \dots & \dots & \dots \\ L^*_{\text{real}[n]} & a^*_{\text{real}[n]} & b^*_{\text{real}[n]} \end{bmatrix} \tag{9}$$

Application of Color Correction and Selection of Cyanosis Region of Interest (ROI): As for the following step, CCM retrieved from the prior step was embedded into the infant's photograph captured earlier. The image of baby's lip and the mouth from the corrected baby image were cropped from the frame using the Crop Tool in Wolfram Mathematica 11.0 to make the ROI selection easier. See Figure 4.



Fig. 4. Instances of cropped images after correction

From the cropped image outcomes, the occurrence of cyanosis at ROI was opted. Since the objective selection of the ROI of cyanosis is challenging, a consistent and repeatable ROIs measurement is obtained by selecting some anthropometric landmarks as depicted in Figure 5. In the facial region, especially in the cyanosis's ROI, there are 6 major landmarks as graphically shown in below figure based on standard face landmarks used in face anthropometry, as recommended in [11].

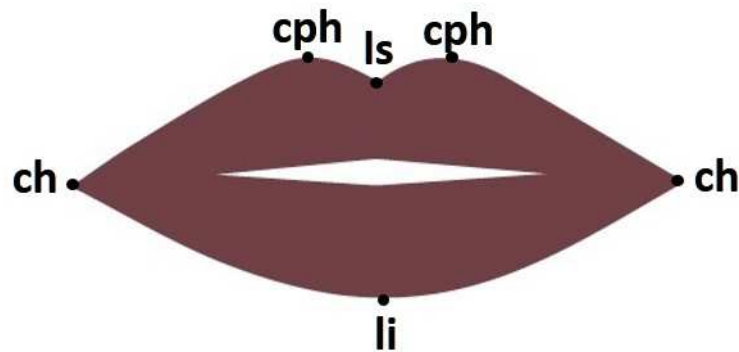


Fig. 5. Facial soft tissue landmarks employed in this study

The abbreviation 'ch' refers to 'cheilion', 'cph' denotes 'crista philtri', 'ls' reflects 'labiale superius', and 'li' means 'labiale'. In fact, the areas pointed in the image had been identified manually, as also performed by [9]. The landmarks in this image were manually identified on each facial scan as marked and the definition of each anthropometry terms are described in Table 1.

8 Azmi *et al.***Table 1.** Definitions of anthropometric landmarks identified on facial scans

Abbreviation	Definition
ch	The point at each labial commissure
cph	The point on each elevated margin of the philtrum above the vermilion line
ls	The midpoint of the upper vermilion line
li	The midpoint of the lower vermilion line

Afterward, by using the landmarks in Figure 5, the Line Segment function in Drawing Tools in Mathematica 11.0 was employed to draw the outer line of the lip which is referred to the central cyanosis region as mention in [19]. Besides, the inner line of the lip is drawn by double-clicking the Line Segment function again to draw the multiple curves. A binarized image of cyanosis's ROIs was created by applying the Binarize function. Next, the function of ImageMultiply had been employed in combining the masks to develop masks of lips, as portrayed in Figure 6. After that, the values of correction color areas were computed.

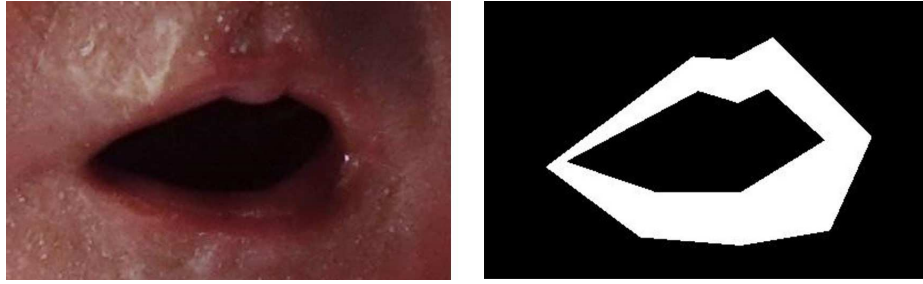


Fig. 6. Right: The cropped image of ROI of cyanosis. Left: Applying the mask to the selected ROI.

1.3 Correction Algorithm Validation

Quantitative validation: The mean value of perceptual color distance between 2 colors, ΔE^*_{ab} was calculated to determine the quality of the suggested algorithm for color correction. Besides, ΔE^* was applied to find the distance between 2 colors [16]. Hypothetically, low value of ΔE^* signifies the difference that reflects nearer to the actual color. In fact, $\Delta E^* > 1$ means color visible to trained eye [3]. The average value of ΔE^* was calculated by identifying the distance of Euclidean from colorchecker to average color from patch. The distance of Euclidean, ΔE^*_{ab} is given below:

$$\Delta E^*_{ab} = \frac{1}{24} \sum_{i=1}^{24} \sqrt{(L^*_a - L^*_b)^2 + (a^*_a - a^*_b)^2 + (b^*_a - b^*_b)^2} \quad (10)$$

The validation defined by calculating the mean and SD of the Euclidean distance of every color patch in the original MacBeth colorchecker compared to before correction color value, as well as the Euclidean distance between after color correction compared to the original MacBeth colorchecker CIELAB values. The results from the Euclidean distances are tabulated in Table 2. The findings showed that prior to correction of color, a vast variation in distance between the colors, in comparison to the actual values of CIELAB, had been observed. In addition, small SD was noted after the correction was performed due to the successful implementation of algorithm for correction. Furthermore, the value of mean after applying color correction substantially decreased by twofold, when compared to the average value prior to correction. Hence, the values after correction are closer to the values determined via X-Rite Ci60 portable spectrophotometer.

Table 2. CIELAB color distances measured on the twenty-four patches before and after correction.

CIELAB color distance	Max	Mean	SD
Before Correction	27.35	18.94	6.18
After Correction	12.30	9.94	1.40

Qualitative validation: Further evaluation was carried out subjectively by comparing the distance of colors in the patches of MacBeth colorchecker (original), photographed images, and images after correction. The after correction image of 24 color patches of the MacBeth colorchecker were regenerated based on corrected color values obtained after color correction was done, as depicted in Section 1.2.2. Figure 7(a) displays the 24 color patches that reflect the actual color in MacBeth colorchecker, which was measured using the X-Rite Ci60 Portable Spectrophotometer. Figure 7(b) refers to the original color of MacBeth colorchecker, measured by X-Rite Ci60 Portable Spectrophotometer, whereas Figure 7(c) exhibits the MacBeth colorchecker after color correction algorithm was performed. The purpose of this validation is to convince the users that the color difference between before and after color correction can be qualitatively assessed.

The amount of contrast or the distance of luminance between 2 colors, ΔL^* gives the visually significant information in luminance difference between 2 colors. In (11) and (12), ΔL^*_{ref} , ΔL^*_{ccp} and ΔL^*_{real} reflect the values of luminance for the actual MacBeth colorchecker, image, and the corrected image in coordinates of the Cartesian system, respectively. In this equation, ΔL^* was subtracted by 100 (luminance value of white) to see the quantity in lightness because it is hard to recognize the difference in black (when L is near to zero). The result of the color difference in the luminance, ΔL^*_{a-b} , between Figure 7(a) and 7(b) is portrayed in Figure 7(d).

$$\Delta L^*_{a-b} = 100 |\Delta L^*_{ref} - \Delta L^*_{ccp}| \quad (11)$$

On the other hand, the equation of ΔL^*_{a-c} between Figures 7(a) and 7(c) as signified in Figure 7(e) shows in the next equation.

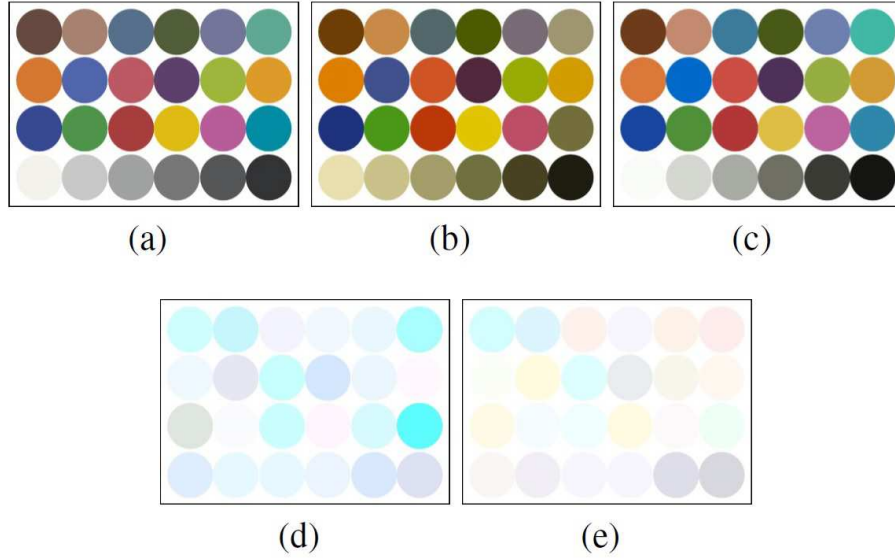


Fig. 7. The images of 24 patches of MacBeth colorchecker: (a) the original color, (b) measured from the image, before color correction was applied, (c) after the correction of the image. The color difference between the original and the measured color values is graphically denoted in (d), while the color difference between the original and the after correction color values is denoted in (e)

$$\Delta L^*_{a-c} = 100 |\Delta L^*_{\text{ref}} - \Delta L^*_{\text{real}}| \quad (12)$$

The validation that was performed qualitatively based on the results of correction has confirmed the efficacy of the proposed system for color correction. When the difference in luminance is small and near to zero which is almost white in color and cannot be recognised by users, then the error of the fitting will be minimum [10]. In other words, the whiter the ΔL^* , the better the results are. The color correction performance was visually verified by the lightness difference between before and after color correction, refers to Figure 7 (e) which nearly cannot be recognised. The color patches are almost white in color as ΔL^* are small and close to 0. However, this kind of assessment can be compromised by the limitations of the printer used.

2 APPLICATION TRIAL

2.1 The imaging system

The imaging tool employed in this work refers to a noncalibrated Sony Cyber-shot DSC-RX 100 type III [4]. During the photography phase, the MacBeth colorchecker chart was placed near the baby on the procedure table in order to make sure both baby and the calibrated object were under the same lighting condition. The colorchecker consists of a cardboard sheet with a matrix of twenty-four colored squares. It was used

as a color reference for image color correction. Besides, it is represented to known colors of objects such as skin, foliage, and sky and 6 grey scale patches [18]. Moreover, information regarding the angle of lighting upon the subject, the distance between light source and subject, as well as the angle of the image captured using camera are absent. Besides, image background and the lighting setting were beyond control.

2.2 Subject

Images of newborn infants were captured in the operation room (OR) of the Máxima Medical Center, Veldhoven, The Netherlands. The methods used in this study were applied to the photos of full-term Caucasian infants, after a Caesarean section (C-section). Delivery via C-sect was selected in this work to gain permission of photography for assessment using colorchecker mainly due to the predetermined delivery time and date. Figure 8 and 9 illustrate two sets of images which were photographed within ten minutes after birth under the standard illuminant in the OR. Each set of images is of one baby only. This study was reviewed by the ethical commission of the MMC Veldhoven and all the parents have given consent for using the pictures. The discoloration in the skin of infants was noted and the results were further confirmed by neonatologist involved in the process of delivery.

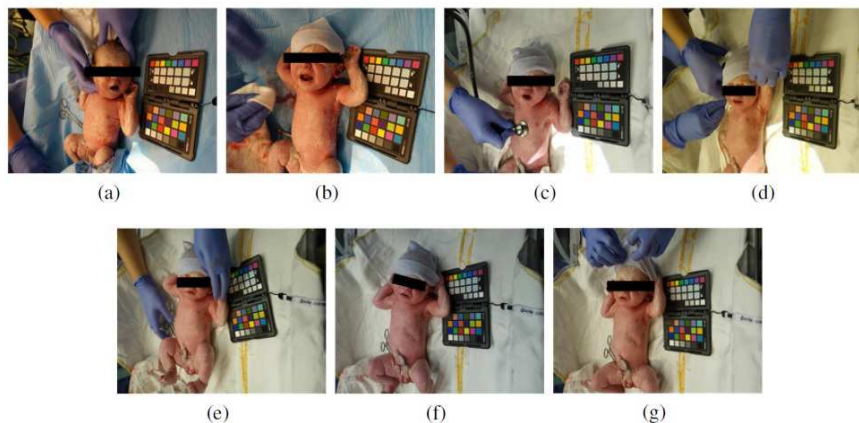


Fig. 8. Example of the first dataset of non-corrected baby images. In a sequence of (a) to (g) visually observed by the clinician as cyanosis to the non-cyanosis skin, respectively

2.3 Method and materials

Next, the system was employed to define cyanosis ROI, as depicted in ROI's section. The unwanted parts of the images were cropped from the images and only significance areas of cyanosis remained back. After that, correction of color was initiated, based



Fig. 9. Example of the second dataset of non-corrected babyimages. In a sequence of (a) to (h) visually observed by the clinician as skin cyanosis to non-cyanosis, respectively

on the correction matrix attained in CCM calculation section. As for this step, all images were corrected first, and later masks of lips were embedded to the images.

The last step for the system that detects cyanosis for images of infants is identifying values of L^* , a^* and b^* for every corrected cyanosis ROI images. Besides, the values of CIELAB for both skin cyanosis and non-cyanosis skin of each L^* , a^* and b^* had been calculated.

2.4 Experimental Results and Discussion

Figure 10 illustrates the scatter plot for CIELAB in $a^* - b^*$ plane. Besides, the shift in color from (1a) to (1g) and (2a) to (2e) were sequenced of baby's skin from cyanosis to non-cyanosis. As noted, the shift in color was observed in $a^* - b^*$ plane, which is from dark brown shade to orange red shade, as portrayed in the chromaticity plot of CIELAB.

Figure (1a) and (2a) in Figure 10 were taken right after delivery of newborn, which indicate breathing without any aid. The skin redness (changes in a^*) was expected to increase from the cyanosis skin color which is blueish to normal healthy skin color and the result was consistent with our expectation.

Figure 10, also projects the color range for color-corrected cyanosis ROI, where the a^* value for the 2 datasets increased from 15.20 (1a) to 28.52 (1g) for the initial dataset, whereas from 19.60 (2a) to 30.54 (2e) for the second dataset. Here, the increasing in a^* value determine the perceptions of health from faces of human skin [24]. In a similar way, the value of b^* increased to 31.05 (1g) from 15.18 (1a) for the initial dataset, while increment in b^* increased from 15.11 (2a) to 32.95 (2h), for the second dataset.

From the results, the coloration from cyanosis to non-cyanosis showed the non-linear pattern as a^* and b^* values had been noted in between (1a) and (1g) and between (2a) and (2h) were fluctuated until reach the highest value in both a^* and b^* .

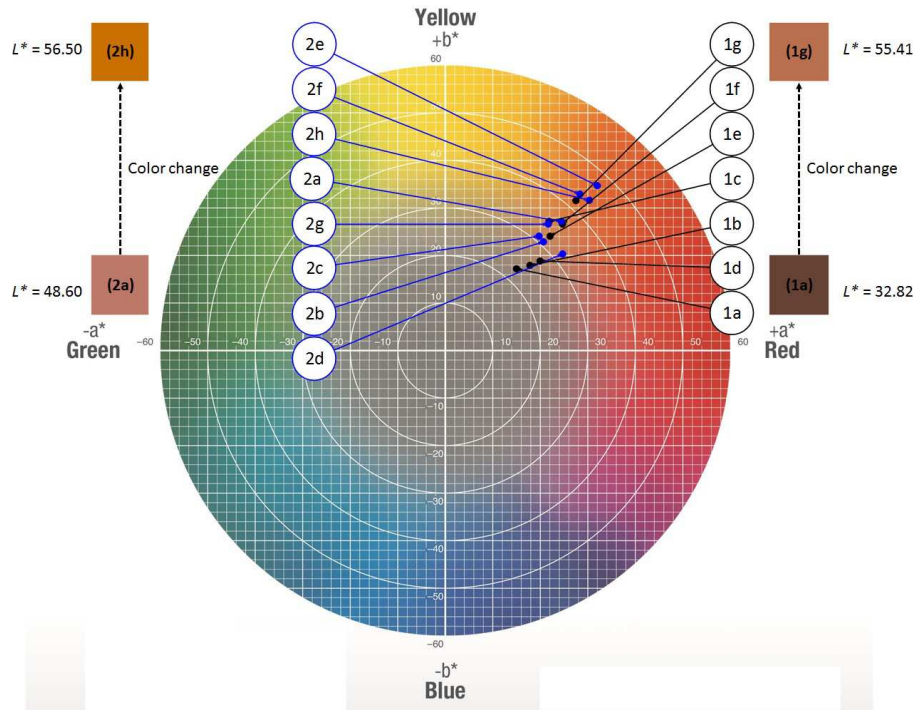


Fig. 10. A result of the changes of a^* and b^* value of the newborn's lip color presented in CIE 1976 $L^*a^*b^*$ color space simulated by the developed color correction system from cyanosis to non-cyanosis color: (1a) to (1f) in the black circle refer to the first images dataset. And the corresponding image from (2a) to (2g) in blue refer to the second dataset of newborn image dataset. The sequence from (a) to (g) are from cyanosis to non-cyanosis state, respectively

In fact, the highest a^* and b^* values had been noted in (1g) and (2h). This also portrays that the value at its highest reflects blood high in oxygen, which explains the condition of lips found in (1g) and (2h), which appear to be the reddest from the rest.

Additionally, both image datasets in this study showed the increment in the L^* value. The increased of L^* value on the chromaticity plane, illustrated by the dash-dotted line on Figure 10. Furthermore, images of (1a) and (2d), which portray post-correction for lip cyanosis, signified values at their lowest for L^* ; 32.82 and 48.60, respectively. On the other hand, images of (1g) and (2e) for lips that are non-cyanosis display values at their highest for L^* , 55.41 and 56.50, respectively in CIELAB color space. Interestingly, the shared similarity between the outcomes of this work and those published in [6] for skin cyanosis and non-cyanosis is indeed astonishing.

Hence, it can be concluded that the shift in color from cyanosis to that of non-cyanosis reflects the transformation of shades from dark brown to orange red in the CIELAB chromaticity plot. However, such finding was not tested in a statistical manner as this work only incorporated 2 datasets of images. Nonetheless, the results

14 Azmi *et al.*

derived from this work are indeed valuable to quantify the cyanosis coloration in image of newborns.

3 CONCLUSION AND FUTURE WORK

The present cyanosis detection method in the baby images with a color correction scheme represent the stepping stone in the development of designing a baby manikin with cyanosis coloration. The obtained results provide a quantitative measure of the color error between the before and after correction baby images. This color correction results are applied to the cyanosis ROI in the images, and a good qualitative and quantitative agreement is found when the data are presented in CIELAB color space. In addition, the chromaticity coordinates is used to differentiate the lips image with and without cyanosis. Besides, determination of cyanosis based on values of CIELAB led to generation of a bigger database of infant images, which can be applied to develop a baby manikin.

Finally, the design of a user-interface can be carried out in order to support selection of ROI, along with development of a database with infant images. This particular work contributes significantly to a neonatal assessment and training for newborn assessment as well as an important step towards the scientific contribution of realistic simulation babies. Besides, this proposed system will facilitate the collection of a reusable example-set of cyanosis and non- cyanosis baby photos for training aids to assess newborns in a more objective manner. Moreover, a stronger basis for subjective way of assessing newborns is developed. No change in illumination conditions are necessary, nor standardized or a very expensive camera is needed.

Looking into future research, more validation could be embedded with inclusion of more images of newborns with varied cases of cyanosis discoloration and babies of various skin color types. In addition, investigation should be carried out to determine the recovery period from cyanosis to non- cyanosis coloration, which now can be measured objectively, by correlating with several other essential functions and future outcomes.

Acknowledgements

The authors would like to express their gratitude and special acknowledgements to Universiti Teknikal Malaysia Melaka (UTeM) and Ministry of Higher Education, Malaysia (KPT) for the funding of the Ph.D. program of Nur Fatimah Azmi and also to the Department of Neonatology M'axima Medical Center, Veldhoven, The Netherlands.

References

1. Basics of color perception and measurement. [online], Availableat:<http://studylib.net/doc/8432172/basics-of-colorperception-and-measurement>
2. Ci6x series portable spectrophotometers. x-rite homepage. [online], Available:[http://www.xrite.com/Ci6x\(2016\)](http://www.xrite.com/Ci6x(2016))
3. Colorwiki - delta e: The color difference [online]. available:, <http://www.colorwiki.com/wiki/DeltaE>.

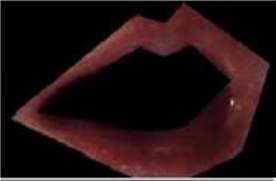
	Before correction	After correction	ΔE^*
(a)			8.45
(b)			11.83
(c)			10.05
(d)			7.54
(e)			9.19
(f)			14.93
(g)			17.63

Fig. 11. The first dataset of before and after color- correction lip images. The corresponding image from (a) to (h) are the image sequence from cyanosis to non-cyanosis state, respectively. The average ΔE^* for this image dataset is 11.38

16 Azmi *et al.*

4. Sony cyber-shot dsc-rx100 digital camera. sony homepage. [online]., <https://www.sony.com>
5. Wolfram mathematica (version 11.0). [online], Available:<https://www.wolfram.com>
6. Azmi, N.F., Delbressine, F., Feijs, L.: Conceptual determination and assessment of cyanosis. *International Journal of Bioscience, Biochemistry and Bioinformatics* 6(3), 75 (2016)
7. Blake, D.: Do we assess 'colour' appropriately using the apgar score? *Journal of Neonatal Nursing* 16(4), 184–187 (2010)
8. Dain, S.J.: Recognition of simulated cyanosis by color-vision-normal and color-vision-deficient subjects. *JOSA A* 31(4), A303–A306 (2014)
9. Djordjevic, J., Pirttiniemi, P., Harila, V., Heikkinen, T., Toma, A.M., Zhurov, A.I., Richmond, S.: Three-dimensional longitudinal assessment of facial symmetry in adolescents. *The European Journal of Orthodontics* 35(2), 143–151 (2011)
10. Everett, J.S., Budescu, M., Sommers, M.S.: Making sense of skin color in clinical care. *Clinical nursing research* 21(4), 495–516 (2012)
11. Farkas, L.G., Deutsch, C.K.: Anthropometric determination of craniofacial morphology. *American Journal of Medical Genetics Part A* 65(1), 1–4 (1996)
12. Hardeberg, J.Y.: Acquisition and reproduction of color images: colorimetric and multispectral approaches. Universal-Publishers (2001)
13. Malacara, D.: Color vision and colorimetry: theory and applications (2003)
14. Marino, B.S., Fine, K.S.: Blueprints pediatrics, vol. 6. Lippincott Williams & Wilkins (2013)
15. Martin, L., Khalil, H.: How much reduced hemoglobin is necessary to generate central cyanosis? *Chest* 97(1), 182–185 (1990)
16. Mokrzycki, W.S., Tatol, M.: Colour difference ΔE -a survey. *MGV* 20(4), 383–411 (2011)
17. Morgan, E.A., Brown, A.: Cyanosis of the new-born. *Journal of the American Medical Association* 105(14), 1085–1088 (1935)
18. Pascale, D.: Rgb coordinates of the macbeth colorchecker. The BabelColor Company pp. 1–16 (2006)
19. Sasidharan, P.: An approach to diagnosis and management of cyanosis and tachypnea in term infants. *Pediatric Clinics* 51(4), 999–1021 (2004)
20. Seo, I., Liu, Y., Bargo, P.R., Kollias, N.: Assessing human skin with diffuse reflectance spectroscopy and colorimetry. In: *Photonic Therapeutics and Diagnostics VIII*. vol. 8207, p. 82070P (2012)
21. Steinhorn, R.H.: Evaluation and management of the cyanotic neonate. *Clinical pediatric emergency medicine* 9(3), 169–175 (2008)
22. Weatherall, I.L., Coombs, B.D.: Skin color measurements in terms of cielab color space values. *Journal of investigative dermatology* 99(4), 468–473 (1992)
23. Wolf, S.: Color correction matrix for digital still and video imaging systems. National Telecommunications and Information Administration (2003)